UC San Diego

UC San Diego Previously Published Works

Title

B Cells Improve Overall Survival in HPV-Associated Squamous Cell Carcinomas and Are Activated by Radiation and PD-1 Blockade

Permalink

https://escholarship.org/uc/item/4bf5m0q6

Journal

Clinical Cancer Research, 26(13)

ISSN

1078-0432

Authors

Kim, Sangwoo S

Shen, Sarek

Miyauchi, Sayuri

et al.

Publication Date

2020-07-01

DOI

10.1158/1078-0432.ccr-19-3211

Peer reviewed

eScholarship.org Powered by the California Digital Library
University of California

Author Manuscript

Author Manuscript

Author Manuscript

Author Manuscript

HHS Public Access

Author manuscript

Clin Cancer Res. Author manuscript; available in PMC 2021 January 01.

Published in final edited form as:

Clin Cancer Res. 2020 July 01; 26(13): 3345–3359. doi:10.1158/1078-0432.CCR-19-3211.

B-cells improve overall survival in HPV-associated squamous cell carcinomas and are activated by radiation and PD-1 blockade.

Sangwoo Shawn Kim[1,2], **Sarek Shen**[2,3], **Sayuri Miyauchi**[1], **Philip Dominick Sanders**[1], **Ida Franiak-Pietryga**[1], **Loren K. Mell**[1], **J. Silvio Gutkind**[4], **Ezra E.W. Cohen**[5], **Joseph Califano**[3], **Andrew B. Sharabi**[1,*]

[1]Department of Radiation Medicine and Applied Sciences, Moores Cancer Center, University of California, San Diego.

[2]School of Medicine, University of California, San Diego

[3]Department of Surgery, Division of Otolaryngology, University of California, San Diego.

[4]Department of Pharmacology, University of California, San Diego.

[5]Department of Medicine, Division of Hematology-Oncology, University of California, San Diego.

Abstract

Purpose: Characterize the role of B-cells on HPV-associated cancer patient outcomes and determine the effects of radiation and PD-1 blockade on B-cell populations.

Experimental Design: Tumor RNA sequencing data from over 800 HNSCC and cervical cancer patients, including a prospective validation cohort, was analyzed to study the impact of B-cell gene expression on overall survival. A novel murine model of HPV+ HNSCC was used to study the effects of PD-1 blockade and RT on B-cell activation, differentiation, and clonality including analysis by single-cell RNA sequencing and B-cell receptor sequencing. Human protein microarray was then used to quantify B-cell mediated IgG and IgM antibodies to over 16,000 proteins in the serum of patients treated on a clinical trial with PD-1 blockade.

Results: RNA sequencing identified CD19 and IGJ as novel B-cell prognostic biomarkers for 3-year overall survival (HR = 0.545, $p < 0.001$). PD-1 blockade and RT enhance development of memory B-cells, plasma cells, and antigen-specific B-cells. B-cell receptor sequencing found that RT enhances B-cell clonality, decreases CDR3 length, and induces B-cell somatic hypermutation.

[*]Corresponding author Andrew B. Sharabi, University of California, San Diego, Moores Cancer Center, Radiation Medicine and Applied Sciences, 3855 Health Sciences Drive, MC 0843, La Jolla, CA 92093, Sharabi@ucsd.edu.

Author Contributions: S.S.K., S.S., S.M., and I.F.P. conducted the experiments and analyzed data. P.D.S., L.K.M., J.S.G., E.E.W.C., and J.A.C. provided administrative, technical, or material support and provided critical review. S.S.K. and A.B.S. designed the experiments and wrote the manuscript. A.B.S. was responsible for research supervision, coordination, and strategy.

Conflict of Interest Statement: LM reports research funding from Merck and Astrazeneca and consulting fees and honoraria from Merck, Pfizer, and Varian Medical Systems. J.S.G reports research funding from Kura Oncology and Mavupharma, and consultant fees from Oncoceutics Inc and Vividion Therapeutics outside the submitted work. E.E.W.C reports research funding from Pfizer, Merck, AstraZeneca, and Bristol-Myers Squibb outside the submitted work. A.B.S. reports research funding and honoraria from Pfizer and Varian Medical Systems, consultant fees from Astrazeneca, and other fees from Raysearch and Merck. A.B.S. is the scientific founder and has an equity interest in Toragen Inc. outside the submitted work. The terms of this arrangement have been reviewed and approved by the University of California, San Diego in accordance with its conflict of interest policies.

Author Manuscript Author Manuscript Author Manuscript Author Manuscript

Single-cell RNA sequencing identified dramatic increases in B-cell germinal center formation after PD- 1 blockade and RT. Human proteome array revealed enhanced IgG and IgM antibody responses in patients who derived clinical benefit but not those with progressive disease after treatment with PD-1 blockade.

Conclusions: These findings establish a key role for B-cells in patient outcomes and responses to PD-1 blockade in HPV-associated squamous cell carcinomas and demonstrate the need for additional diagnostics and therapeutics targeting B-cells.

Introduction

The essential role that the immune system plays in tumor control is now at the forefront of oncology, and understanding how innate and adaptive anti-tumor responses work in concert is vital to improving the efficacy of immunotherapy (1,2). Many studies evaluating anti-tumor immune responses have focused on T-cells and myeloid cells; however, the role of B-cells in oncology has been studied much less frequently. There exist multiple distinct subsets of human B-cells including B-cell progenitors, immature B-cells, plasma cells, memory B-cells, and immunosuppressive or regulatory B-cells (B-regs) (3,4). In addition, formation of germinal centers is the hallmark of B-cell mediated adaptive immunity and is required for proper B-cell affinity maturation and antibody diversification (5). While B-cells are principally known for humoral immune responses, the function of B-cells that migrate and infiltrate into primary tumors remains poorly understood.

In melanoma, B-cell depletion was associated with decreased local tumor control, increased lung metastases, and impaired tumor-antigen specific CD8+ T cell proliferation (6). A recent report has shown that tumor-associated B-cells may play a role in maintaining inflammatory responses in melanoma (7). In head and neck squamous cell carcinoma (HNSCC), an early study of 33 patients did not observe an association between tumor infiltrating immune cells at the primary site and patient outcomes, but did demonstrate improved outcomes with increased peritumoral B-cells in lymph node metastases (8). Recent analyses of B-cell phenotypes and responses in HNSCC described significant heterogeneity; however, the effect of B-cells on survival or responses to immunotherapy or radiation was not explored (9,10). Conversely, other studies have described an immunosuppressive or protumorigenic role for B-cells including a subset of IL-10-producing B-regs (11-13), and B-cells have been implicated in contributing to chronic inflammation that can then lead to de novo carcinogenesis in squamous cell carcinomas (14). Recently, two studies have described a major role of B-cells in melanoma and soft-tissue sarcomas in mediating responses to immunotherapy, however the role of B-cells in HNSCC, and the effect of specific treatment regimens, including PD-1 blockade and RT, on modulating B-cell populations remains largely unknown (15,16).

Anti-PD-1/PD-L1 checkpoint blockade immunotherapy (CBI) is approved for metastatic squamous cell carcinomas including HNSCC, cervical cancer, and lung cancer (17-19). For HNSCC, radiation therapy (RT) and RT combined with concurrent chemotherapy are two of the most effective treatment options and a standard of care for locally advanced disease (20). Importantly, HPV-associated squamous cell carcinomas are among the most rapidly rising

Author Manuscript Author Manuscript Author Manuscript Author Manuscript

cancer types and it is estimated that 4.5% of all cancers worldwide are attributable to HPV(21). However, the mechanisms underlying the efficacy of radiation therapy in HNSCC, in particular for HPV+ tumors, are not entirely understood (22,23). Recent preclinical studies examining combinations of RT and CBI have described synergistic effects, and multiple ongoing clinical trials are evaluating this combination in locoregionally advanced squamous cell carcinomas (24-29). Our group was one of the first to demonstrate that PD-1 blockade and RT can enhance B-cell mediated IgG anti-tumor antibody responses in melanoma (27); however, the effects of these therapies in squamous cell carcinomas and on B-cell subpopulations which express PD-1 and PD-L1 themselves remains unclear.

Here, we first analyzed pre-treatment tumor RNA-sequencing data from over 800 patients and found that high expression of two B-cell specific markers results in dramatically improved 3-year overall survival (OS). We then analyzed the effects of B-cells on tumor control and the impact that CBI and RT can have on B-cells in squamous cell carcinomas using HNSCC as a model. We found significant changes in B-cell activation, differentiation, and memory formation after treatment with CBI and RT. Single-cell RNA sequencing demonstrated striking increases in germinal formation with CBI and RT. Furthermore, we demonstrate that CBI and RT induce dramatic increases in IgG and IgM antibody levels in patients with anti-tumor responses but not in those with progressive disease. This report characterizes the changes in B-cell populations induced by PD-1 blockade and RT and correlates these B-cell specific genes with survival in HNSCC and cervical squamous cell carcinomas.

Materials and Methods

Mouse strains and cell lines

C57BL/6 female 6-week-old mice were purchased from The Jackson Laboratory. C3H female 6-week-old mice were purchased from Charles River. AT-84-E7 cells were kindly obtained from Dr. Aldo Venuti (Regina Elena National Cancer institute; Italy), and were used to generate a line of OVA-expressing cells, termed AT-84-E7-OVA. OVA ORF was cloned into MSCV-Blasticidin vector and construct was confirmed by DNA sequencing. HEK293T cells were co-transfected with MSCV-Blasticidin-OVA and Ecopac (pIK6.1MCV.ecopac.UTd) using PEI reagent (Sigma). Retroviruses from the culture medium were then used to infect AT-84-E7 cells, and underwent selection with blasticidin (6 μg/ml) to establish a stable cell line. After drug selection, AT-84-E7-OVA was cultured in RPMI 1640 media supplemented with 10% FBS, 1% L-Glutamine, 1% Penicillin/Streptomycin, 1% Sodium Pyruvate, Geneticin (200 μg/ml), and blasticidin (3 μg/ml). OVA expression was verified by Western Blotting prior to expansion. B16-OVA melanoma cells were obtained from Dr. Hyam Levitsky (Johns Hopkins University) and cultured in RPMI 1640 media supplemented with 10% FBS, 1% L-Glutamine, 1% Penicillin/Streptomycin, 1% Sodium Pyruvate, and Geneticin (200 μg/ml). All tumor cell lines were tested for *Mycobacterium* intermittent and found to be free of *Mycobacterium* prior to *in vivo* use in mice.

Author Manuscript Author Manuscript Author Manuscript Author Manuscript

Flow cytometry, cell surface staining, and TIL preparation

Single-cell suspensions were generated from spleens, inguinal lymph nodes, and tumors. To isolate tumor-infiltrating lymphocytes (TIL), density gradient centrifugation using an 80%/40% Percoll (GE Healthcare) gradient was done on the single-cell suspensions from excised tumors. Cells were then stained with fluorophore-conjugated antibodies from BioLegend and BD Biosciences and analyzed using an LSR II flow cytometer (BD Biosciences). Antibodies against the following cell surface markers (clone) were used: CD19 (6D5), B220 (RA3–6B2), IgD (11–26c.2a), IgM (RMM-1), IgG (Poly4053), CD80 (16–10A1), MHC II (M5/114.15.2), CD27 (LG.3A10), PD-L2 (TY25), CD1d (1B1), CD5 (53–7.3), CD138 (281–2), CD45.2 (104). Additionally, a live/dead Zombie Yellow stain and fluorophore-conjugated streptavidin with biotinylated-ovalbumin at approximately 1:10 molar ratio were used. For the apoptosis assay, a flow cytometry-based kit (BioLegend) utilizing Annexin V, propidium iodide, and select cell surface markers were used following manufacturer's protocol. Flow cytometry data were then analyzed using FlowJo v10 (BD).

Antigen-multimer generation

OVA purchased from Sigma-Aldrich was biotinylated and isolated using the EZ-Link NHS-PEG4 Biotinylation Kit from ThermoFisher Scientific per kit protocol. Biotinylation of the OVA protein was successively verified using a 4'-hydroxyazobenzene-2-carboxylic acid (HABA) assay. Biotinylated-OVA was then stored at −80° C until use.

Serum OVA antibody analysis

Mouse whole blood was collected by cardiac puncture at the time of euthanization. Serum was isolated by allowing whole blood to coagulate at room temperature for 90 minutes prior to centrifugation at 1000 g for 20 minutes. Serum supernatant was then collected and stored at −80° C. Serum OVA antibodies were analyzed using an in-house generated anti-Ovalbumin total IgG (mouse) ELISA assay. In brief, plates were loaded with 1 ug OVA protein per well and incubated overnight at 4° C. Plates were then washed the next day and blocked with PBS + 2% bovine serum albumin for 2 hours. Sera were then diluted 1:100 prior to loading onto the ELISA plate for 1 hour. Secondary rabbit anti-mouse antibody conjugated to HRP was then added and incubated for 30 minutes. TMB reagent was then added and then quenched with 2.5M HCl. Absorbance at 450 nm was then read using a TECAN infinite M200 plate reader. Standard murine anti-OVA IgG antibody (3G2E1D9) were used to generate titration curves.

Tumor growth experiments, anti-PD-L1 therapy, radiation therapy

B16-OVA and AT-84-E7-OVA cells were cultured and injected subcutaneously in the right flank with 1.5 × 10^5 cells (B16-OVA) or 5 × 10^5 cells (AT-84-E7-OVA) on day 0. The injection sites were monitored until a tumor was palpable. The tumor was then measured using electronic calipers every 3 days and tumor volume was calculated using $(l \times \hat{w}2)/2$. Anti-PD-L1 therapy and RT was started as soon as tumors were palpable. Mice were treated with 200 μg anti-PD-L1 antibody (BioXcell) via intraperitoneal injections every 3 days for a total of 3 injections per mouse. Mice were treated with 12–18 Gy of focal radiation to the tumor site using a JL Shepherd Cs-137 Irradiation (JL Shephard and Associates, San

Author Manuscript Author Manuscript Author Manuscript Author Manuscript

Francisco, CA) a dose rate of 2.53 Gy / min. To direct radiation, customized lead shielding with a jig to immobilize the region receiving radiation were used for each mouse. To deplete B-cells, 250 μg of anti-CD20 antibody (clone SA271G2, Biolegend) was given intravenously through the tail vein following manufacturer instructions 5 days prior to tumor injection.

B-Cell Sorting, Single-Cell RNA-Sequencing Library Preparation, and Sequencing

B-cells from inguinal or tumor-draining lymph nodes were pooled from 3 different mice to obtain single-cell suspensions. Cells were then stained with fluorophore-conjugated antibodies from BioLegend and sorted on a FACSAria cell sorter. Antibodies against the following cell surface marker (clone) were used: CD19 (1D3/CD19), CD45.2 (104), CD3e (145–2C22), Gr-1 (RB6–8C5), CD11b (M1/70), TER-119 (TER-119). Cells were additionally stained with propidium iodide. Following sorting, cells were counted using an Invitrogen Countess II FL and loaded into the 10x-Genomics Chromium controller. 10x-Genomics v3 libraries were then prepared as per manufacturer recommendations. Initial quality control was done using a Qubit 2.0 Fluorometer. Libraries were then sequenced aiming for a minimum coverage of 20000 reads per cell using an Illumina HiSeq 4000 at the Institute for Genomic Medicine at the University of California, San Diego. Single-cell RNA sequencing data were initially analyzed using Cell Ranger (10x Genomics) and converted into matrix files. The data were then subsequently analyzed using Seurat v3.(49,50)

B-Cell Receptor Sequencing

VDJ recombination sequencing analysis was performed by Adaptive Biotechnologies (Seattle, WA) on genomic DNA isolated from tumor-draining lymph nodes and tumors. DNA was extracted using a Qiagen DNeasy kit per kit protocol. For the sequencing analysis, libraries were prepared by multiplex PCR to cover all possible IgH rearrangements, followed by high-throughput sequencing of CDR3 of the B-cell receptor. Data were initially visualized and analyzed using the ImmunoSEQ Analyzer.

HuProt Proteome Microarray Analysis

Patient sera were collected from consented patients under a University of California, San Diego Human Research Protections Program Institutional Review Board approved protocol (HRPP# 151570). The study was conducted in accordance with ethical principles from the Declaration of Helsinki. Sera were analyzed using the HuProt Proteome Microarray v3.1 (CDI Laboratories, Inc). In brief, sera were diluted 1:1000 before incubating on a slide with >15,000 GST-tagged human proteins. Following sera incubation, a fluorophore-conjugated secondary antibody recognizing either IgG or IgM was added prior to plate reading.

Patient HNSCC and Cervical Cancer Tumor RNA Sequencing Analysis

Patient HNSCC tumor RNA sequencing data were obtained from the TCGA and a prospectively collected, proprietary, curated database of HPV+ HNSCC from Johns Hopkins University (JHU). Patient cervical cancer tumor RNA sequencing data were obtained from the TCGA, TCGA RNASeq data was obtained from the National Cancer Institute Genomic

Author Manuscript Author Manuscript Author Manuscript Author Manuscript

Data Commons (http://portal.gdc.cancer.gov/). Thresholds for determining “high” vs “low” expression were set at both the median and 75th percentile of gene reads.

Statistics

Statistical analysis was performed using Prism 7 (GraphPad) and R. One-way ANOVA with a Tukey’s post-hoc test for multiple comparisons were conducted for flow cytometry and BCR sequencing analysis. Cox proportional hazard models were used to characterize the difference between gene expression levels in patient survival analysis. The effect of clinical, demographical, and gene expression levels on 3-yr OS was assessed using multivariate logistic regression. All data are shown as mean +/− SEM. Results were considered significant if $P \leq 0.05$ (*), 0.01 (**), 0.001 (***).

Study Approval

Patients in the JHU cohort were recruited under protocol NA_00–36235, which was approved by the JHU IRB. Patients in the University of California, San Diego (UCSD) cohort were recruited under IRB approved protocol UCSD HRPP 151570 (ClinicalTrials.gov Identifier: NCT02843165). Animal experiments were performed at the University of California, San Diego Moores Cancer Center under protocols approved by the Institutional Animal Care and Use Committee (IACUC) Office.

Results

RNA sequencing analysis demonstrates clear survival advantage with high expression of B-cell specific markers in squamous cell carcinomas

To study the importance of B-cells in survival of patients with HPV+ squamous cell carcinomas, we analyzed B-cell specific genes in tumor samples from The Cancer Genome Atlas (TCGA) RNA sequencing (RNA-Seq) database. CD19 is a coreceptor for the B-cell receptor and is a canonical B-cell marker (30). Based on *CD19* expression, we divided all TCGA head and neck squamous cell carcinoma (HNSCC) patients into either high-expressing or low-expressing relative to median expression (Supplementary Table 1). We did observe baseline differences between these groups with an increased percentage of HPV+ oropharyngeal subsite patients in the *CD19*-high cohort. When stratifying all patients by *CD19* status, we observed a dramatic increase in 3-year overall survival (OS) in patients with high expression of *CD19* (Fig. 1A). There was a median survival of 5.65 years in *CD19*-high patients vs 2.70 years in *CD19*-low patients [3-year OS hazard ratio (HR) of 0.545; 95% confidence interval (CI) 0.41–0.72; $P<0.001$]. *CD19*-high patients had 3-year survival rates of 68.9% (95% CI 0.63–0.76) compared to 47.4% (95% CI 0.41–0.55) in CD*19*-low patients. When stratifying by HPV status, we found HPV- *CD19*-low patients also had worse survival, and that HPV+ *CD19*-low patients had an unexpected dramatically worse survival (Fig. 1B and Supplementary Figure 1A). These findings demonstrate the impact of *CD19* B-cell expression on outcomes regardless of HPV status.

As HPV+ oropharyngeal subsite patients are known to have improved outcomes compared to HPV- patients, we performed multivariate logistic analysis of survival based on *CD19* expression controlling for clinical-pathological features including HPV status, smoking

Author Manuscript Author Manuscript Author Manuscript Author Manuscript

status, disease subsite, TNM stage, and *CD8* or *CD45* expression status amongst others (Supplementary Table 2, 3). *CD8* and *CD45* expression status were separately included to control for an inflamed tumor microenvironment. On multivariate analysis *CD19* expression remained highly significant, and above-median expression was protective, with a 3-year OS HR of 0.58 ($P = 0.001$) and 0.55 ($P = 0.003$) when accounting for *CD8* and *CD45* expression, respectively. Univariate regression analyses for individual variables used in the multivariate analysis are shown in Supplementary Table 4. Intriguingly, *CD19* was shown to be a stronger predictor for overall survival than either *CD8* or *CD45* expression status, supporting the independent prognostic capacity of *CD19* expression as a biomarker for survival in HNSCC. Moreover, there was a significant interaction between *CD19* expression and HPV status such that *CD19* expression level has an *increased* effect size in stratifying survival in HPV+ patients compared to HPV- patients (Fig 1. and Supplementary Table 5). Thus, pre-treatment CD19 expression is highly prognostic of OS independent of anatomic subsite, HPV status, and clinical stage, and may reflect the underlying biology of HNSCC tumors.

While the expression of *CD19* indicates the presence of B-cells, we wanted to confirm these findings with additional B-cell specific genes. The *IGJ* gene (also referred to as *JCHAIN*) encodes the J-chain, an adaptor protein for IgM and IgA antibodies, and is one of the most specific B-cell markers (31). In all HNSCC cases, there was a median survival of 7.40 years for *IGJ*-high patients vs 3.91 years for *IGJ*-low patients (3-year OS HR of 0.49; 95% CI of 0.34–0.70; $P<0.001$) (Fig 1E). *IGJ*-high patients had a 3-year survival rates of 74.8% (95% CI 0.67–0.84) compared to 52% (95% CI 0.47–0.58) for *IGJ*-low patients. Analysis of survival by HPV status and *IGJ* expression are shown in Figures 1F and Supplementary Figure 1B. Multivariate analysis was repeated and demonstrated a significant correlation with 3-year OS with a HR of 0.70 (P = 0.001) and 0.57 ($P = 0.002$) when accounting for *CD8* and *CD45* expression, respectively; complete results are shown in Supplementary Tables 6 and 7. Additionally, we analyzed the effect of multiple B-cell genes involved in development, differentiation, and memory formation on overall survival using both median and 75th percentile gene expression cutoffs to define high vs low expression (10). We found that high expression of multiple B-cell genes correlated with improved survival, and these results calculating 3-year OS HR using both thresholds of median and 75th percentile expression levels are summarized in Supplementary Table 8.

In order to cross-validate these findings in a different HPV-related malignancy we performed a similar analysis of TCGA data from cervical cancer patients. We observed no baseline differences in various clinical-pathologic variables in patients classified as being *CD19*-high vs *CD19*-low (Supplementary Table 9). Similar to HNSCC, high expression of either *CD19* or *IGJ* was associated with improved overall survival in cervical cancer patients compared to those who had low expression of *CD19* or *IGJ*, respectively (Fig 1C, G).

Prospective analysis confirms survival advantage with CD19 and IGJ B-cell markers in independent HPV+ validation cohort.

To further validate these findings, we analyzed an independent dataset of prospectively-collected tumor RNA-Seq data from 35 HPV+ HNSCC patients (Supplementary Table 10).

Author Manuscript Author Manuscript Author Manuscript Author Manuscript

In this validation dataset, we observed concordant increases in survival in patients with high expression of *CD19* [HR 0.23; 95% CI 0.06–0.95; $P = 0.049$) (Fig 1D) or *IGJ* [HR 0.25; 95% CI 0.06–0.997; $P = 0.058$) (Fig 1H). Taken together, these findings identify *CD19* and *IGJ* as novel B-cell biomarkers that are highly prognostic of 3-year overall survival in patients with squamous cell carcinomas. Importantly, while HPV+ patients are known to have a better overall prognosis compared to HPV- patients, *CD19* or *IGJ* expression was able to stratify HPV+ patients biologically into $CD19^{high}$HPV+ patients with an excellent prognosis, and $CD19^{low}$HPV+ patients with a dramatic and unexpected worse prognosis.

B-cell depletion promotes tumor growth

To analyze the functionality of B-cells in HNSCC and effects of treatment we used the AT-84-E7 murine model (32). AT-84-E7 is an HPV-oncogene expressing syngeneic HNSCC model derived from oral squamous mucosa of the C3H mouse (32), which was also engineered to express OVA (AT-84-E7-OVA). We found that treatment with anti-PD-L1 CBI alone did not significantly decrease tumor growth while RT led to reduced tumor growth, and the addition of anti-PD-L1 CBI to RT (referred to as “combined therapy”) further improved tumor control (Fig 2A). To evaluate the effect of B-cell function on local tumor control, mice were treated with anti-CD20 antibody intravenously to deplete peripheral B-cells (33). Mice were treated 5 days prior to tumor injection to ensure that B-cells were depleted prior to tumorigenesis to mitigate the early effects of B-cell immunity derived from injection. We found that B-cell depleted mice developed larger tumors with a faster tumor growth velocity than matched control mice (Fig 2C). Additionally, B-cell depleted mice trended to having larger tumor size after treatment with RT, anti-PD-L1 CBI, or combined therapy (Supplementary Figure 2).

Anti-PD-L1 immunotherapy and radiation therapy enhance B-cell maturation and activation

Next, we used multiparametric flow cytometry to further analyze the impact of CBI and RT on B-cell phenotypes. We analyzed surface expression of MHC II on mature (IgD^+, IgM^{low}), transition type 1 (T1; IgD^-IgM^+), and transitional type 2 (T2; IgD^+IgM^{high}) B-cells in the TDLN of AT-84-E7-OVA tumor-bearing mice by looking at geometric mean fluorescence index (gMFI). (Fig 2D). A schematic of the full gating strategy used is provided in Supplementary Figure 3. MHC II expressed on B-cells is important for its antigen presenting capabilities to $CD4^+$ T cells and successive differentiation and effector functions (34,35). In the TDLN, combined therapy led to the greatest increase in surface MHC II in mature and T2 B-cells, while in T1 B-cells, anti-PD-L1 CBI was associated with the highest MHC II expression (Fig 2E). In the spleen, a similar analysis found that RT paradoxically decreased MHC II expression in T1 and T2 B-cells, and this was rescued with combined therapy (Supplementary Figure 4A,B)

To examine these findings in a different model system and mouse background, we repeated these experiments using a B16-OVA melanoma model in C57BL/6 mice. Combined therapy led to the greatest local tumor control as previously shown (Fig 2B) (36). In the TDLN, we identified mature, T1, and T2 B-cells (Fig 2F), and there were concordant findings with combination therapy leading to the greatest increase in MHC II expression across all B-cells (Fig 2G). On splenic B-cells in this system, we found that combined therapy led to the

Author Manuscript Author Manuscript Author Manuscript Author Manuscript

highest upregulation of MHC II across all B-cells (Supplementary Figure 4C,D). Overall, these data demonstrate RT can prime mature B-cells and skew them towards a more activated state, and anti-PD-L1 CBI can augment this effect.

PD-1 Blockade Can Reverse Radiation-Induced Increases in Regulatory B-Cells

We next examined immunosuppressive regulatory B cells (B-regs) in the TDLN. As described by Yanaba et al., B-regs were identified as $CD1d^{High}CD5^{+}$, and secrete IL-10 to inhibit T cell-dependent responses; there was also a distinct population of $CD1d^{Low}CD5^{+}$ whose relevance is not clearly defined (11). We applied this gating strategy to $CD19^{+}B220^{+}$ lymphocytes (Fig 2H). In the TDLN in both the AT-84-E7-OVA and B16-OVA models, RT increased $CD1d^{High}CD5^{+}$ B-regs, however, this increase was abrogated with combined therapy (Fig 2I). As RT was associated with increased B-regs in the TDLN, there may be a negative effect of RT alone in inducing immunosuppressive cells, that can be partially reversed with the addition of PD-1 blockade. This ability for PD-1 blockade to mitigate the increase in B-regs due to RT alone is analogous to what we observed for $CD4^{+}CD25^{+}Foxp3^{+}$ regulatory T cells in the tumor (27). The ability for RT to induce immunosuppressive T-regulatory cells has been reported by multiple groups; however, this is the first report to our knowledge demonstrating that RT alone can induce B-reg populations (27,37).

Radiation Increases Tumor Antigen-Specific B-Cells and Plasma Cell Differentiation

In order to analyze antigen defined B-cells using our AT-84-E7-OVA model we generated an “OVA-Multimer” reagent by biotinylating OVA molecules and staining with a fluorophore-conjugated streptavidin molecule to identify B-cells possessing B-cell receptors (BCRs) that recognize OVA. We observed that B-cells possessing BCRs that bind OVA could be divided into IgG+ and IgG- (Fig 3A). When analyzing IgG+ cells in the TDLN, there were dramatic changes to antigen-specific B-cells as RT alone significantly increased the proportion of $IgG^{+}OVA\text{-}Multimer^{+}$ B-cells (Fig 3B). Interestingly, the addition of anti-PD-L1 CBI appeared to blunt this increase, perhaps due to relative changes in other B-cell populations, which can downregulate BCR upon activation. Interestingly, we did not observe any increase in $OVA\text{-}Multimer^{+}$ B-cells in the spleen, which may be related to differences in antigen-processing and capture in the TDLN versus spleen (Supplementary Figure 5A). When tested in a B16-OVA model, similar effects to the populations of $IgG^{+}OVA\text{-}Multimer^{+}$ B-cells in the TDLN and spleen were observed (Fig 3C, D and Supplementary Figure 5B).

To study the effect of CBI and RT on B-cell plasma cell differentiation from $CD19^{+}IgD^{-}$ lymphocytes, we analyzed $CD138^{+}IgG^{+}$ and $CD138^{+}IgG^{-}$ subsets. CD138 is a canonical marker for plasma cells and is a member of the heparan sulfate proteoglycan family involved in many cellular pathways, including cellular adhesion (38). In both AT-84-E7-OVA and B16-OVA models, mice that were treated with combined therapy exhibited a significant increase in $CD138^{+}IgG^{+}$ plasma cells in the TDLN (Fig 3E). In the spleen, combined therapy similarly significantly increased populations of $CD138^{+}IgG^{+}$ plasma cells in both AT-84-E7-OVA and B16-OVA models (Fig 3F). In order to account quantify absolute counts of plasma cells, we irradiated spleens with 8Gy or 20Gy and confirmed an increase in absolute count of plasma cells in the spleen, which supports our findings of increased

Author Manuscript Author Manuscript Author Manuscript Author Manuscript

frequency of plasma cells induced with radiation therapy (Supplementary Figure 5C). To quantify changes in B-cell mediated humoral antibody responses, we measured concentrations of antibodies against OVA and confirmed that mice bearing B16-OVA tumors treated with combined therapy had the highest anti-OVA antibody concentrations (Fig 3G). Taken together, these data indicate that anti-PD-L1 CBI and RT can increase B-cell differentiation into plasma cells and enhance B-cell mediated antigen-specific antibody responses.

PD-1 Blockade and radiation modulate development of B-cell memory cells in the Tumor-Draining Lymph Node

Memory B-cell subsets are rare populations, which can dramatically expand upon exposure to cognate antigen. To analyze memory B-cells, we use a combination of CD80, PD-L2, and surface expression of IgG and IgM to identify four distinct B-cell memory subsets: IgG $^{+}$CD80^{-}PD-L2^{+} (IgG^{+} Single Positive [SP]), IgG^{+}CD80^{+}PD-L2^{+} (IgG^{+} Double Positive [DP]), IgG^{-}IgM^{+}CD80^{-}PD-L2^{+} (IgM^{+} SP), and IgG^{-}IgM^{+}CD80^{+}PD-L2^{+} (IgM^{+} DP) as defined by Zuccarino-Catania et al. (Fig 3H) (39). In the TDLN of the AT-84-E7-OVA model, treatment with RT led to a dramatic increase in the populations of IgG^{+} SP and DP memory B-cells, and this was augmented in mice that received combined therapy (Fig 3I). In the spleen, combined therapy led to decreased IgG^{+} and IgM^{+} SP memory B-cells (Supplementary Figure 6A).

Similarly, in the B16-OVA model, combination therapy resulted in the greatest increased IgG^{+} SP memory B-cells (Fig 3J, left). RT itself increased IgM^{+} SP memory B-cells, and this was not significantly altered with combined therapy (Fig 3J, right). In the spleen of these mice, combined therapy led to the highest increases in the populations of IgG^{+} SP and IgM^{+} SP B-cells (Supplementary Figure 6). The modulation of only a subpopulation of memory B-cell populations demonstrates the differential effect of RT and anti-PD-L1 CBI on B-cells and warrants further investigation into the molecular mechanisms modulating memory development.

Differential Radiosensitivity of B-Cell Subsets

Next, we investigated whether specific B-cell subsets had variable radiosensitivity by irradiating spleens of wild type mice and analyzing apoptosis *ex-vivo* of CD19+B220+ cells using a combination of propidium iodide (PI) and Annexin V (AnnV). We quantified the proportion of cells that were live (PI^{-}AnnV^{-}), undergoing early apoptosis (PI^{-}AnnV^{+}), and undergoing late apoptosis (PI^{+}AnnV^{+}). We observed that CD19+B220+ B-cells in general are susceptible to undergoing apoptosis by 20Gy (Fig 3K). Non-class switched memory B-cells showed an increased susceptibility to apoptosis at 8Gy and 20Gy, while plasma cells has a non-significant increase in apoptotic cells (Fig 3L, M). This suggests that B-cells are susceptible to radiation induced apoptosis, and specific subsets possess differential radiosensitivity.

Author Manuscript Author Manuscript Author Manuscript Author Manuscript

BCR Sequencing Demonstrates Changes to B-Cell Repertoire and Clonality Due to Radiation and Anti-PD-L1 CBI

To characterize changes in the antigen repertoire of B-cells, we performed BCR sequencing on matched TDLN and tumor in mice bearing AT-84-E7-OVA tumors treated with CBI and/or RT. Within all TDLN samples, there were multiple shared B-cell clones across treatment groups (Fig 4A). Productive templates, defined as sequences that are in-frame and do not contain a stop codon, can be assayed using BCR sequencing. Mice treated with RT had a lower number of total productive templates, but higher fraction of productive templates in the TDLN (Supplementary Figure 7A, B). Importantly, we observed an increase in productive clonality, which measures the clonality of productive templates, and maximum productive frequency in mice treated with RT alone. The addition of RT to anti-PD-L1 CBI significantly increased productive clonality but not maximum productive frequency (Fig 4B, C).

We next looked at somatic hypermutation (SHM), which is a critical process for affinity maturation of germinal center B-cells. Anti-PD-L1 CBI or RT alone did not significantly alter the mean number of SHM in each productive BCR sequence; however, mice treated with combined therapy had more SHM per productive sequence (Fig 4D).

BCR sequencing of tumor samples demonstrated less drastic changes to B-cell phenotype, likely due to the lower frequency of tumor-infiltrating B-cells. There was a trend towards increased total productive templates and productive clonality in mice treated with RT alone (Supplementary Figure 7D, E). RT alone significantly increased maximum productivity frequency, whereas RT and anti-PD-L1 CBI alone but not in combination increased mean number of SHM (Supplementary Figure 7F, G).

Radiation Therapy Drives Changes in BCR CDR3 Loop Length

On average mature B-cells that have undergone affinity maturation and antigen selection have BCRs with shorter CDR3 regions than immature B-cells (40). We observed that in the TDLN, RT alone decreased the mean CDR3 loop length (Supplementary Figure 7C). Mice treated with combined therapy had a mean CDR3 loop length that was similar to mice treated with RT alone but statistically lower than mice treated with anti-PD-L1 CBI alone. When calculating the fraction of BCR sequences with CDR3 loops less than 12 amino acids, mice treated with RT alone had the highest proportion of short CDR3 loops (Fig 4E). In the tumor, we did not observe significant changes in CDR3 loop length based on treatment (Supplementary Figure 7H).

Single cell RNA sequencing reveals distinct subpopulations of B-cells

In order to analyze changes in B-cell subpopulations in further detail we performed single cell RNA-sequencing (scRNA Seq) on fluorescence-activated cell sorted (FACS) B-cells. $CD3^-CD11b^-Gr\text{-}1^-Ter\text{-}199^-CD19+$ B-cells from naïve non-tumor bearing mice, and draining lymph nodes (TDLN) from AT-84-E7-OVA flank tumor-bearing mice treated with anti-PD-L1 CBI, RT, RT combined with anti-PD-L1 CBI and controls, were subjected to scRNA seq. The B-cell sorting procedure as well as quality control measures for sequencing are shown in Supplementary Figure 8. We first compared all tumor-bearing mice, both as individual

Author Manuscript Author Manuscript Author Manuscript Author Manuscript

data sets and as a single, integrated dataset (Supplementary Figure 9A). Uniform manifold approximation and projection (UMAP) and unsupervised clustering of the integrated data revealed two clearly distinct subsets of B-cells divided into 6 clusters (Fig 5A). These two subsets were found to represent either germinal center (GC) or follicular B-cells based on differential gene expression analysis of genes previously characterized to be up-regulated in GC B-cells, such as *Bcl6*, *Mki67*, and *Aicda* (Fig 5B) (41). We identified 4 unique clusters, named F1-F4, representing follicular B-cells (Fig 5C). Cluster F1 represented naïve follicular B-cells, with increased expression of genes such as *Jun*, *CD55*, and *Vpreb3*. Clusters F2-F4 corresponded to subsets possessing an activated phenotype. Cluster F2 had particularly high expression of *Mif*, a proinflammatory cytokine with chemokine functionality, and *Il4i1*, cluster F3 had increased expression of genes such as *Plac8*, *Fcrl5*, and *Apoe*, and cluster F4 upregulated multiple genes induced by interferon, such as *Ifit3* and *Ifi44*. Next, there were two clusters, named GC1 and GC2, corresponding to GC B-cells. Cluster GC1 was characterized by higher expression of *Sema7a*, *Cd83*, *Cxcr4*, and *Cxcr5*, corresponding to light zone (LZ) GC B-cells, and cluster GC2 was characterized by higher expression of *Mki67* and *Top2a,* corresponding to dark zone (DZ) GC B-cells (Fig 5D); the full list of differentially expressed genes between clusters GC1 and GC2 are provided in Supplementary Data Table 1. The exquisite detail and clustering provided by performing scRNAseq on FACS sorted B-cells serves as a map for further investigation of these distinct B-cell subsets and peripheral subpopulations.

PD-1 Blockade and radiation therapy increase B-cell germinal center formation in the tumor draining lymph node

Given the critical role of germinal centers for B-cell mediated adaptive immune responses, we focused on determining the effects of anti-PD-L1 CBI and radiation on GC clusters. Partitioning of the GC region of the integrated dataset based on treatment demonstrated striking increase in cell density upon treatment, with the highest density in mice receiving combined therapy (Fig 5E). Untreated mice possessed 16.3% GC B-cells. Mice treated with anti-PD-L1 CBI and RT individually possessed 21.0% and 21.9% GC B-cells, respectively, while mice treated with combined therapy had 42.9% of total B-cells in the GC clusters, indicating robust activation of antigen-specific adaptive immune responses with combined therapy (Fig 5F). The relative contribution of LZ and DZ GC B-cells are shown in Supplementary Figure 9B. This clustering and percentages of cells belonging to each GC cluster was consistent between the single and integrated datasets. In comparison, naïve, non-tumor-bearing mice had only 2.1% of total B-cells in the GC cluster, suggesting that the presence of tumor itself increases GC formation (Supplementary Figure 9C).

Closer examination of the GC B-cell cluster revealed two states with expression profiles intermediate of LZ and DZ GC B-cells, which were termed intermediate zone-1 and intermediate zone-2 (Supplementary Figure 10A) (42). Transcriptionally, intermediate zone-1 more closely resembled LZ GC B-cells but had higher expression of *Mki67* and *Top2a*, two markers indicating a proliferative cell phenotype, whereas intermediate zone-2 more closely resembled DZ GC B-cells (Supplementary Figure 10B). The relative distribution of these zones within GC B-cells was similar across treatment groups, indicating that this GC clustering was robust and reproducible (Supplementary Figure 10C). Overall,

Author Manuscript Author Manuscript Author Manuscript Author Manuscript

these data indicate that anti-PD-L1 CBI combined with RT can dramatically promote GC formation in the TDLN and induce development of adaptive B-cell immune responses.

Patients Responding to CBI Demonstrate Increased Antibody Production After Treatment

To characterize the effects of PD-1 blockade on B-cell mediated antibody responses in humans, we used the HuProt proteome microarray to quantify individual IgM and IgG serum antibody responses to over 16,000 proteins in 6 patients with HPV-associated cancers enrolled on a Phase II Randomized Clinical Trial comparing the use of CBI +/− stereotactic body radiation therapy (SBRT) in patients with advanced metastatic cancer (UCSD HRPP 151570; ClinicalTrials.gov Identifier: NCT02843165). Clinical and pathologic details of all patients analyzed are shown in Supplementary Table 11. We compared baseline pretreatment sera to sera collected 2 months after treatment and determined fold-changes in both IgG and IgM antibody responses against each protein in the array. Importantly during an initial humoral immune response for thymus-dependent antigens, multimeric IgM antibodies predominate prior to class switching, affinity maturation, and development of a robust IgG response. We defined two distinct regions: region 1 represents antigens that elicited an increased IgG to IgM relative fold-change after treatment, which we term “secondary antibody response antigens” and region 2 represents antigens that elicited an increased IgM to IgG relative fold-change after treatment which we term “primary antibody response antigens”. To isolate targets that had significantly increased fold-change in antibodies, a fold-change of 8 was used as a threshold. Representative antibody profiles are shown in Figure 6.

We observed that patients with objective responses to therapy (Fig 6A,B) had dramatically increased IgG and IgM responses post-treatment (Region 1 and Region 2) compared to patients with progressive disease (Fig 6C,D). The absolute number of antigens recognized in each region for each patient is also included in Supplementary Table 11. The fluorescence value changes for the top 25 or fewer targets in in each region for each representative patient is shown for IgG – region 1 (Fig 6E) and IgM – region 2 (Supplementary Figure 11A). Finally, we compared the number of highly elevated IgG and IgM responses (>8 fold change) in patients with a clinical benefit to therapy versus those with progressive disease. Clinical benefit was defined as a complete response, objective partial response, or stable disease lasting greater than 6 months. We found that patients with a clinical benefit from PD-1 blockade had remarkably increased absolute number of IgG and IgM responses with >8 fold change compared to patients with progressive disease (Fig 6F).

Conclusions / Discussion

B-cells are a critical arm of the adaptive immune system and play dual roles as both professional antigen presenting cells and specialized antibody-producing cells. Although they are not known to have direct cytotoxic capability, understanding how B-cells contribute to a multifaceted immune response targeting tumor-associated antigens or tumor-associated viruses is vital. Our data support an anti-tumorigenic role of B-cells in HPV-related squamous cell carcinomas and a remarkably beneficial impact on patient outcomes. Fortunately, HPV+ HNSCC patients are known to have improved outcomes compared to

Author Manuscript Author Manuscript Author Manuscript Author Manuscript

HPV- patients, although the reasons behind this are not fully understood and additional biomarkers are needed to help stratify these populations. Currently the only biological prognostic marker in widespread clinical use is p16, which is a surrogate marker of HPV positivity in oropharyngeal HNSCC. Importantly, the *CD19* and *IGJ* biomarkers reported here remained significant for OS on multivariate analysis, demonstrating that analysis of the underlying biology within HNSCC tumors adds significant prognostic value beyond HPV or p16 status. Interestingly, we observed an *increased* effect size and a statistical interaction between CD19/IGJ and HPV-positivity when compared to HPV-negative HNSCC patients. This finding suggests a biological interaction between B-cells and the human papilloma virus and perhaps reflects the importance of B-cells reacting against HPV-associated antigens.

Among HPV-positive patients there is known to be significant heterogeneity and HPV-positive subpopulations have been identified with disparate clinical outcomes (43,44). Zhang et al., identified two subtypes of HPV-related HNSCC – one characterized by expressing genes involved in immune responses and mesenchymal differentiation that trended towards a better prognosis, and the other expressing genes involved in keratinocyte differentiation and cell adhesion (44). However, as opposed to hierarchical clustering based upon a large number of various genes, we were able to stratify our HPV+ patients based upon expression of a single B-cell marker, supporting the key role that B-cells play in squamous cell carcinomas and highlighting the potential clinical convenience of a single gene test. Additionally, because our analyses were performed on pre-treatment biopsies, these B-cell specific markers have the potential to guide biologically driven management protocols in the future, for example, to escalate therapy in high-risk patients or de-escalate therapy in biologically defined low-risk patients. Moreover, in addition to HNSCC and cervical cancer these B-cell markers may play important roles in other HPV-associated malignancies including anal, penile, or vulvar cancer. Further investigation into the predictive capacity of these B-cell markers in prospective clinical trials is certainly deserved.

In light of the association between B-cells and survival, the ability of PD-1 blockade or RT to modulate B-cell development and function is of paramount importance and likely plays a role in the clinical activity of these therapies. We present a comprehensive approach to characterizing B-cells in both a murine model and human patients, including scRNA-seq, flow cytometry, BCR sequencing, and antibody profiling. Using scRNA-sequencing on sorted B-cells we identified enhanced germinal center formation due to PD-1 blockade and RT. Thus, this is direct evidence that PD-1 blockade and radiation can enhance development antigen specific B-cells. We confirmed this by developing a novel ‘OVA-multimer’ reagent to track antigen specific B-cells and demonstrated that combined therapy increased plasma cell differentiation and resultant anti-OVA IgG antibody levels. Analogous to tetramers for T-cells, this novel and unique OVA-multimer reagent could be used generally to quantify antigen specific B-cell populations in other model systems.

Complementing flow cytometry, B-cell receptor sequencing is a powerful new technology that allows for exquisite characterization B-cell clonal diversity. B-cell clones that recognize a specific set of antigens proliferate in the lymph node and germinal center, altering clonality, although analysis of clonality in B-cells has the additional complexity of somatic

Author Manuscript Author Manuscript Author Manuscript Author Manuscript

hypermutation. In support of this, we also observed a significant decrease in CDR3 length after RT, which is known to correlate with antigen-specific responses(40). Interestingly, we did not observe a significant increase in clonality with CBI alone. The reasons behind his finding remain unclear; although, the PD-1 receptor is known to have important regulatory functions on B-cells (45) and PD-L1-high B-cells are key regulators of humoral immune responses (46). One possibility is that PD-1 blockade alone does not significantly enhance antigen presentation or that the timing of the effects of PD-1 blockade on tumor cell death and B-cell mediated antigen processing is delayed compared to RT. These BCR sequencing findings certainly deserve further investigation in patients especially in light of the important prognostic information gained from human TCR sequencing (47).

Ultimately, the major effector function of B-cells is antibody production and the ability for CBI to modulate changes in B-cell mediated antibody levels is understudied. The two novel regions that we defined have important implications. Region 1 which we term ‘secondary antibody response antigens’ which have developed predominant IgG responses after class switching; and Region 2 which we term ‘primary antibody response antigens’ in which IgM responses dominate prior to class switching (or due to antigens which do not elicit class switching) and represent de-novo immune responses induced during treatment. For example, Patient 3, who had HNSCC that completely responded to combined CBI and SBRT, demonstrated increased antibodies against ANP32A, a target in HNSCC that is associated with increased mortality in patients with N0 and N1 disease (48). Taken together these findings demonstrate that CBI can induce anti-tumor antibodies and patients with objective responses to therapy demonstrate a profound humoral response pattern, which may play a key role in tumor control. As we analyzed a limited number of patients, a larger cohort is needed to comprehensively characterize changes in antibody profiles based upon responses. Nevertheless, the regions defined here provide a novel framework for characterizing enhancements in pre-existing humoral immunity (Region 1) versus development of de-novo antibodies (Region 2) after initiation of CBI. Further analyses of these distinct regions in relation to response patterns as well as immune related adverse events and novel tumor antigens is deserved.

In summary, we report that CD19 and IgJ are B-cell specific prognostic biomarkers for survival in HNSCC and cervical squamous cell carcinomas. The ability of these single gene markers to further stratify patient outcomes beyond HPV status is powerful and has implications for personalized management. The observed inferior tumor control in mice whose peripheral B-cells have been depleted demonstrates a key role for B-cells in HNSCC tumor control. Furthermore, the ability of CBI and RT to modulate B-cell activation and germinal center formation provides evidence of systemic B-cell changes that shape adaptive immune responses and may play a role in clinical activity of these therapies. Finally, the identification of distinct regions of IgG versus IgM endogenous antibody responses which develop after CBI provides a novel framework for understanding how B-cell antibodies contribute to patient outcomes and correlate with responses to PD-1 blockade. Cumulatively, these data reveal a remarkably underappreciated role for B-cells in squamous cell carcinomas and provide strong rationale for using B-cell markers to stratify patients and developing novel therapeutics targeting B-cell populations.

Author Manuscript Author Manuscript Author Manuscript Author Manuscript

Supplementary Material

Refer to Web version on PubMed Central for supplementary material.

Acknowledgements:

We thank the La Jolla Institute for Immunology for their Flow Cytometry core. We thank the consultation and services of the Institute for Genomic Medicine and Center for Computational Biology and Bioinformatics at the University of California, San Diego. We additionally thank Dr. Hyam Levitsky (Johns Hopkins University, Baltimore, Maryland) for the B16-OVA cell line and Dr. Aldo Venuti (Regina Elena National Cancer Institute, Roma, Italy) for the AT-84-E7 cell line. This work was supported in part by 1KL2TR001444, R01 DE028563, and 1U01 DE028227-01.

References:

1. Couzin-Frankel J Breakthrough of the year 2013. Cancer immunotherapy. Science 2013;342(6165):1432–3 doi 10.1126/science.342.6165.1432. [PubMed: 24357284]
2. Kaiser J, Couzin-Frankel J. Cancer immunotherapy sweeps Nobel for medicine. Science 2018;362(6410):13 doi 10.1126/science.362.6410.13. [PubMed: 30287641]
3. Blair PA, Norena LY, Flores-Borja F, Rawlings DJ, Isenberg DA, Ehrenstein MR, et al. CD19(+)CD24(hi)CD38(hi) B cells exhibit regulatory capacity in healthy individuals but are functionally impaired in systemic Lupus Erythematosus patients. Immunity 2010;32(1):129–40 doi 10.1016/j.immuni.2009.11.009. [PubMed: 20079667]
4. Knippenberg S, Peelen E, Smolders J, Thewissen M, Menheere P, Cohen Tervaert JW, et al. Reduction in IL-10 producing B cells (Breg) in multiple sclerosis is accompanied by a reduced naive/memory Breg ratio during a relapse but not in remission. Journal of neuroimmunology 2011;239(1–2):80–6 doi 10.1016/j.jneuroim.2011.08.019. [PubMed: 21940055]
5. Mesin L, Ersching J, Victora GD. Germinal Center B Cell Dynamics. Immunity 2016;45(3):471–82 doi 10.1016/j.immuni.2016.09.001. [PubMed: 27653600]
6. DiLillo DJ, Yanaba K, Tedder TF. B cells are required for optimal CD4+ and CD8+ T cell tumor immunity: therapeutic B cell depletion enhances B16 melanoma growth in mice. Journal of immunology (Baltimore, Md : 1950) 2010;184(7):4006–16 doi 10.4049/jimmunol.0903009.
7. Griss J, Bauer W, Wagner C, Simon M, Chen M, Grabmeier-Pfistershammer K, et al. B cells sustain inflammation and predict response to immune checkpoint blockade in human melanoma. Nat Commun 2019;10(1):4186 doi 10.1038/s41467-019-12160-2. [PubMed: 31519915]
8. Pretscher D, Distel LV, Grabenbauer GG, Wittlinger M, Buettner M, Niedobitek G. Distribution of immune cells in head and neck cancer: CD8+ T-cells and CD20+ B-cells in metastatic lymph nodes are associated with favourable outcome in patients with oro- and hypopharyngeal carcinoma. BMC Cancer 2009;9:292 doi 10.1186/1471-2407-9-292. [PubMed: 19698134]
9. Lechner A, Schlosser HA, Thelen M, Wennhold K, Rothschild SI, Gilles R, et al. Tumor-associated B cells and humoral immune response in head and neck squamous cell carcinoma. Oncoimmunology 2019;8(3):1535293 doi 10.1080/2162402X.2018.1535293. [PubMed: 30723574]
10. Wood O, Woo J, Seumois G, Savelyeva N, McCann KJ, Singh D, et al. Gene expression analysis of TIL rich HPV-driven head and neck tumors reveals a distinct B-cell signature when compared to HPV independent tumors. Oncotarget 2016;7(35):56781–97 doi 10.18632/oncotarget.10788. [PubMed: 27462861]
11. Yanaba K, Bouaziz JD, Haas KM, Poe JC, Fujimoto M, Tedder TF. A regulatory B cell subset with a unique CD1dhiCD5+ phenotype controls T cell-dependent inflammatory responses. Immunity 2008;28(5):639–50 doi 10.1016/j.immuni.2008.03.017. [PubMed: 18482568]
12. Tang A, Dadaglio G, Oberkampf M, Di Carlo S, Peduto L, Laubreton D, et al. B cells promote tumor progression in a mouse model of HPV-mediated cervical cancer. International journal of cancer 2016;139(6):1358–71 doi 10.1002/ijc.30169. [PubMed: 27130719]
13. Shalapour S, Font-Burgada J, Di Caro G, Zhong Z, Sanchez-Lopez E, Dhar D, et al. Immunosuppressive plasma cells impede T-cell-dependent immunogenic chemotherapy. Nature 2015;521(7550):94–8 doi 10.1038/nature14395. [PubMed: 25924065]

Author Manuscript Author Manuscript Author Manuscript Author Manuscript

14. Andreu P, Johansson M, Affara NI, Pucci F, Tan T, Junankar S, et al. FcRgamma activation regulates inflammation-associated squamous carcinogenesis. Cancer cell 2010;17(2):121–34 doi 10.1016/j.ccr.2009.12.019. [PubMed: 20138013]
15. BA H, SM R, J G, S Z, R B, R T, et al. B Cells and Tertiary Lymphoid Structures Promote Immunotherapy Response. Nature 2020 doi 10.1038/s41586-019-1922-8.
16. F P, A dR, EZ K, TW C, CM S, J C, et al. B Cells Are Associated With Survival and Immunotherapy Response in Sarcoma. Nature 2020 doi 10.1038/s41586-019-1906-8.
17. Ferris RL, Blumenschein G Jr., Fayette J, Guigay J, Colevas AD, Licitra L, et al. Nivolumab for Recurrent Squamous-Cell Carcinoma of the Head and Neck. The New England journal of medicine 2016;375(19):1856–67 doi 10.1056/NEJMoa1602252. [PubMed: 27718784]
18. Seiwert TY, Burtness B, Mehra R, Weiss J, Berger R, Eder JP, et al. Safety and clinical activity of pembrolizumab for treatment of recurrent or metastatic squamous cell carcinoma of the head and neck (KEYNOTE-012): an open-label, multicentre, phase 1b trial. Lancet Oncol 2016;17(7):956–65 doi 10.1016/S1470-2045(16)30066-3. [PubMed: 27247226]
19. Cohen EEW, Soulieres D, Le Tourneau C, Dinis J, Licitra L, Ahn MJ, et al. Pembrolizumab versus methotrexate, docetaxel, or cetuximab for recurrent or metastatic head-and-neck squamous cell carcinoma (KEYNOTE-040): a randomised, open-label, phase 3 study. Lancet (London, England) 2019;393(10167):156–67 doi 10.1016/S0140-6736(18)31999-8.
20. Pignon JP, le Maitre A, Maillard E, Bourhis J. Meta-analysis of chemotherapy in head and neck cancer (MACH-NC): an update on 93 randomised trials and 17,346 patients. Radiother Oncol 2009;92(1):4–14 doi 10.1016/j.radonc.2009.04.014. [PubMed: 19446902]
21. de Martel C, Plummer M, Vignat J, Franceschi S. Worldwide burden of cancer attributable to HPV by site, country and HPV type. International journal of cancer 2017;141(4):664–70 doi 10.1002/ijc.30716. [PubMed: 28369882]
22. Ang KK, Harris J, Wheeler R, Weber R, Rosenthal DI, Nguyen-Tan PF, et al. Human papillomavirus and survival of patients with oropharyngeal cancer. The New England journal of medicine 2010;363(1):24–35 doi 10.1056/NEJMoa0912217. [PubMed: 20530316]
23. Fakhry C, Westra WH, Li S, Cmelak A, Ridge JA, Pinto H, et al. Improved survival of patients with human papillomavirus-positive head and neck squamous cell carcinoma in a prospective clinical trial. J Natl Cancer Inst 2008;100(4):261–9 doi 10.1093/jnci/djn011. [PubMed: 18270337]
24. Chemoradiation vs Immunotherapy and Radiation for Head and Neck Cancer. https://ClinicalTrials.gov/show/NCT03383094.
25. Immunotherapy and SBRT for Metastatic Head and Neck Carcinomas. https://ClinicalTrials.gov/show/NCT03283605.
26. REirradiation and Programmed Cell Death Protein 1 (PD-1) Blockade On Recurrent Squamous Cell Head and Neck Tumors. https://ClinicalTrials.gov/show/NCT03317327.
27. Sharabi AB, Nirschl CJ, Kochel CM, Nirschl TR, Francica BJ, Velarde E, et al. Stereotactic Radiation Therapy Augments Antigen-Specific PD-1-Mediated Antitumor Immune Responses via Cross-Presentation of Tumor Antigen. Cancer Immunol Res 2015;3(4):345–55 doi 10.1158/2326-6066.CIR-14-0196. [PubMed: 25527358]
28. Jie HB, Gildener-Leapman N, Li J, Srivastava RM, Gibson SP, Whiteside TL, et al. Intratumoral regulatory T cells upregulate immunosuppressive molecules in head and neck cancer patients. British journal of cancer 2013;109(10):2629–35 doi 10.1038/bjc.2013.645. [PubMed: 24169351]
29. Mandal R, Senbabaoglu Y, Desrichard A, Havel JJ, Dalin MG, Riaz N, et al. The head and neck cancer immune landscape and its immunotherapeutic implications. JCI insight 2016;1(17):e89829 doi 10.1172/jci.insight.89829. [PubMed: 27777979]
30. Tedder TF, Isaacs CM. Isolation of cDNAs encoding the CD19 antigen of human and mouse B lymphocytes. A new member of the immunoglobulin superfamily. Journal of immunology (Baltimore, Md : 1950) 1989;143(2):712–7.
31. Palmer C, Diehn M, Alizadeh AA, Brown PO. Cell-type specific gene expression profiles of leukocytes in human peripheral blood. BMC Genomics 2006;7:115 doi 10.1186/1471-2164-7-115. [PubMed: 16704732]

Author Manuscript Author Manuscript Author Manuscript Author Manuscript

32. Paolini F, Massa S, Manni I, Franconi R, Venuti A. Immunotherapy in new pre-clinical models of HPV-associated oral cancers. Hum Vaccin Immunother 2013;9(3):534–43 doi 10.4161/hv.23232. [PubMed: 23296123]
33. Moyron-Quiroz JE, Lin L, Oida T, Garcia-Mojica S, Yang X. Kinetic study of B cell-depletion with a novel mAb anti-mouse CD20, clone SA271G2. The Journal of Immunology 2016;196(1 Supplement):209.23-.23.
34. Katikaneni DS, Jin L. B cell MHC class II signaling: A story of life and death. Hum Immunol 2019;80(1):37–43 doi 10.1016/j.humimm.2018.04.013. [PubMed: 29715484]
35. Good-Jacobson KL, Song E, Anderson S, Sharpe AH, Shlomchik MJ. CD80 expression on B cells regulates murine T follicular helper development, germinal center B cell survival, and plasma cell generation. Journal of immunology (Baltimore, Md : 1950) 2012;188(9):4217–25 doi 10.4049/jimmunol.1102885.
36. Sharabi AB, Lim M, DeWeese TL, Drake CG. Radiation and checkpoint blockade immunotherapy: radiosensitisation and potential mechanisms of synergy. Lancet Oncol 2015;16(13):e498–509 doi 10.1016/S1470-2045(15)00007-8. [PubMed: 26433823]
37. Muroyama Y, Nirschl TR, Kochel CM, Lopez-Bujanda Z, Theodros D, Mao W, et al. Stereotactic Radiotherapy Increases Functionally Suppressive Regulatory T Cells in the Tumor Microenvironment. Cancer Immunol Res 2017;5(11):992–1004 doi 10.1158/2326-6066.cir-17-0040. [PubMed: 28970196]
38. O'Connell FP, Pinkus JL, Pinkus GS. CD138 (syndecan-1), a plasma cell marker immunohistochemical profile in hematopoietic and nonhematopoietic neoplasms. Am J Clin Pathol 2004;121(2):254–63 doi 10.1309/617d-wb5g-nfwx-hw4l. [PubMed: 14983940]
39. Zuccarino-Catania GV, Sadanand S, Weisel FJ, Tomayko MM, Meng H, Kleinstein SH, et al. CD80 and PD-L2 define functionally distinct memory B cell subsets that are independent of antibody isotype. Nature immunology 2014;15(7):631–7 doi 10.1038/ni.2914. [PubMed: 24880458]
40. Rosner K, Winter DB, Tarone RE, Skovgaard GL, Bohr VA, Gearhart PJ. Third complementarity-determining region of mutated VH immunoglobulin genes contains shorter V, D, J, P, and N components than non-mutated genes. Immunology 2001;103(2):179–87 doi 10.1046/j.1365-2567.2001.01220.x. [PubMed: 11412305]
41. Meehan TF, Vasilevsky NA, Mungall CJ, Dougall DS, Haendel MA, Blake JA, et al. Ontology based molecular signatures for immune cell types via gene expression analysis. BMC Bioinformatics 2013;14:263 doi 10.1186/1471-2105-14-263. [PubMed: 24004649]
42. Milpied P, Cervera-Marzal I, Mollichella ML, Tesson B, Brisou G, Traverse-Glehen A, et al. Human germinal center transcriptional programs are de-synchronized in B cell lymphoma. Nature immunology 2018;19(9):1013–24 doi 10.1038/s41590-018-0181-4. [PubMed: 30104629]
43. Gleber-Netto FO, Rao X, Guo T, Xi Y, Gao M, Shen L, et al. Variations in HPV function are associated with survival in squamous cell carcinoma. JCI insight 2019;4(1) doi 10.1172/jci.insight.124762.
44. Zhang Y, Koneva LA, Virani S, Arthur AE, Virani A, Hall PB, et al. Subtypes of HPV-Positive Head and Neck Cancers Are Associated with HPV Characteristics, Copy Number Alterations, PIK3CA Mutation, and Pathway Signatures. Clinical cancer research : an official journal of the American Association for Cancer Research 2016;22(18):4735–45 doi 10.1158/1078-0432.CCR-16-0323. [PubMed: 27091409]
45. Thibult ML, Mamessier E, Gertner-Dardenne J, Pastor S, Just-Landi S, Xerri L, et al. PD-1 is a novel regulator of human B-cell activation. Int Immunol 2013;25(2):129–37 doi 10.1093/intimm/dxs098. [PubMed: 23087177]
46. Khan AR, Hams E, Floudas A, Sparwasser T, Weaver CT, Fallon PG. PD-L1hi B cells are critical regulators of humoral immunity. Nat Commun 2015;6:5997 doi 10.1038/ncomms6997. [PubMed: 25609381]
47. Hopkins AC, Yarchoan M, Durham JN, Yusko EC, Rytlewski JA, Robins HS, et al. T cell receptor repertoire features associated with survival in immunotherapy-treated pancreatic ductal adenocarcinoma. JCI insight 2018;3(13) doi 10.1172/jci.insight.122092.

Author Manuscript Author Manuscript Author Manuscript Author Manuscript

48. Velmurugan BK, Yeh KT, Lee CH, Lin SH, Chin MC, Chiang SL, et al. Acidic leucine-rich nuclear phosphoprotein-32A (ANP32A) association with lymph node metastasis predicts poor survival in oral squamous cell carcinoma patients. Oncotarget 2016;7(10):10879–90 doi 10.18632/oncotarget.7681. [PubMed: 26918356]

49. Butler A, Hoffman P, Smibert P, Papalexi E, Satija R. Integrating single-cell transcriptomic data across different conditions, technologies, and species. Nat Biotechnol 2018;36(5):411–20 doi 10.1038/nbt.4096. [PubMed: 29608179]

50. Stuart T, Butler A, Hoffman P, Hafemeister C, Papalexi E, Mauck WM, et al. Comprehensive Integration of Single-Cell Data. Cell 2019;177(7):1888–902.e21 doi 10.1016/j.cell.2019.05.031. [PubMed: 31178118]

Author Manuscript Author Manuscript Author Manuscript Author Manuscript

Translational Relevance:

The human papilloma virus (HPV) is thought to be causative agent for approximately 5% of all cancers worldwide resulting in significant morbidity and mortality. Many studies evaluating immune correlates in the tumor microenvironment have focused T-cells or myeloid cells; however, the role of B-cell populations is rarely studied. Here we discovered a remarkable beneficial role for B-cells in overall survival of patients with squamous cell carcinomas and used cutting edge technologies to comprehensively characterize the effects of PD-1 blockade and radiation therapy on B-cell populations.

Specifically, we have identified CD19 and IGJ as single gene B-cell specific prognostic biomarkers for 3-year overall survival. Furthermore, we discovered that B-cell mediated IgG and IgM antibody responses correlate with response patterns to PD-1 blockade. These data establish a key role for B-cells in HPV-associated squamous cell carcinomas and provide strong rationale for development of additional diagnostics and novel therapeutics targeting B-cells.

Author Manuscript Author Manuscript Author Manuscript Author Manuscript

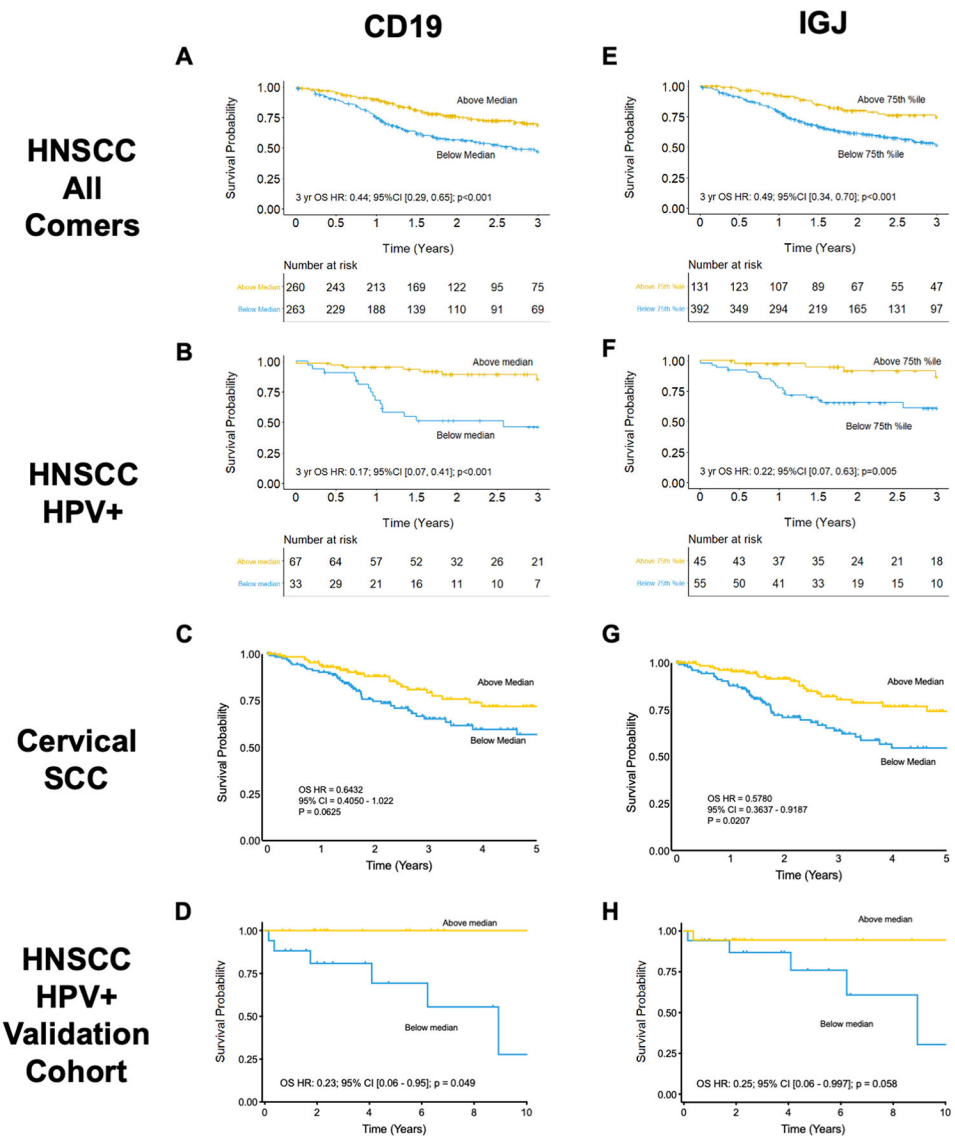

Figure 1: CD19 and IGJ are B-cell specific prognostic biomarkers for overall survival in HPV-associated squamous cell carcinomas.

(A, E) Overall survival analysis based on CD19 and IGJ expression in all TCGA HNSCC cases. (B, F) Subgroup analysis of HPV+ HNSCC cases. (C, G) Overall survival analysis based on CD19 and IGJ expression in all TCGA cervical cancer cases. (D, H) Overall survival analysis based on CD19 and IGJ expression in all HPV+ HNSCC cases in our validation cohort.

Author Manuscript Author Manuscript Author Manuscript Author Manuscript

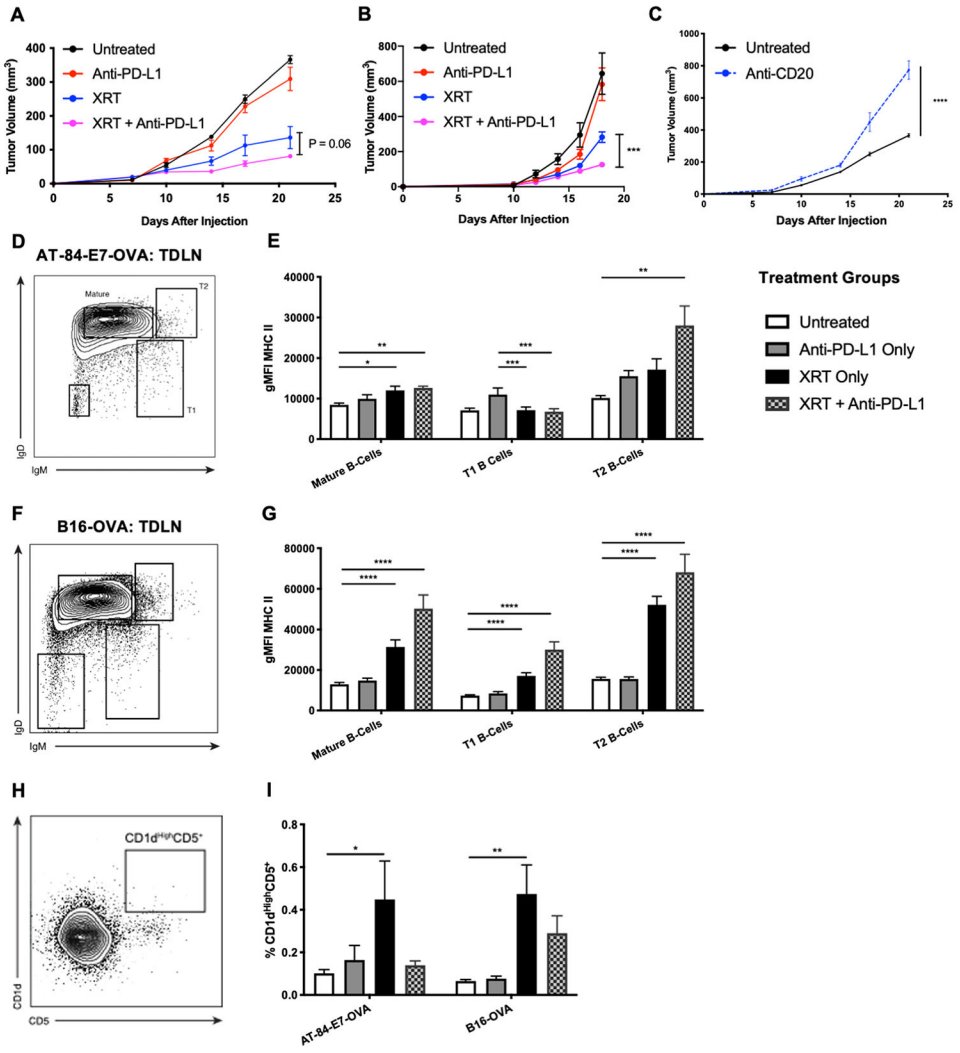

Figure 2: B-cell depletion promotes tumor growth and anti-PD-L1 immunotherapy and radiation therapy modulate B-cell activation.

(A) Tumor volumes of mice (n = 6–7 per group) inoculated with 5×10^5 cells of AT84-E7-OVA tumor cells. Treatment with radiation (12 Gy x 1) and/or anti-PD-L1 CBI (200 μg every 3 days for 3 total doses) beginning on day 6. This experiment was conducted three times with similar results. (B) Tumor volumes of mice (n = 6–7 per group) inoculated with 1×10^5 cells of B16-OVA tumor cells. (C) Tumor volumes of mice (n=5 per group) inoculated with 5×10^5 cells of AT-84-E7-OVA tumor cells. Mice were treated with anti-CD20 antibody to deplete B cells. (D, F) Representative contour plots for IgD and IgM expression to define mature, T1, and T2 B-cells in the TDLN. (E, G) MHC II expression within each subpopulation of B-cells in the TDLN. (H) Representative contour plot and gating schematic for regulatory B-cells in the TDLN. (I) Percent regulatory B-cell (CD1dHigh, CD5+) in the TDLN.

Author Manuscript Author Manuscript Author Manuscript Author Manuscript

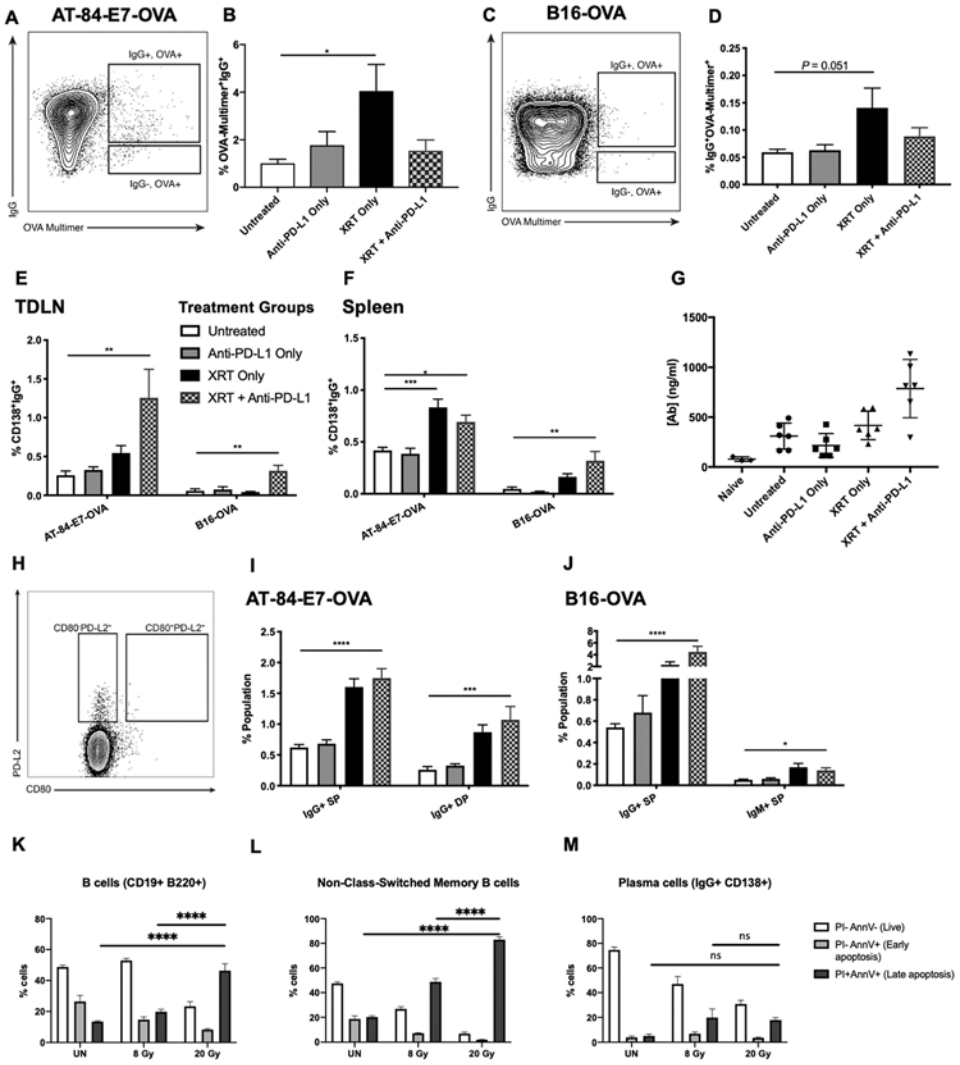

Figure 3: Radiation therapy enhances development of antigen-specific B cells, promotes plasma cell and memory B-cell differentiation, and stimulates antibody production.

(A, C) Representative contour plot of antigen-specific B cells in AT-84-E7-OVA and B16-OVA models. (B, D) Percent IgG+OVA-Multimer+ B-cells in the TDLN. (E, F) Percent plasma cells (CD138+, IgG+) in the TDLN (E) and spleen (F). (G) Antibody concentrations against OVA in B16-OVA bearing mice. (H) Representative contour plot for SP and DP memory populations, gated on IgG+ cells. (I, J) Percent of each memory population in AT-84-E7-OVA-bearing mice (I) and B16-OVA-bearing mice (J). (K-M) Percent of cells in each group that were live (PI-, AnnV-), in early apoptosis (PI-, AnnV+), and in late apoptosis (PI+, AnnV+). Groups contained 6–8 mice per group.

Author Manuscript Author Manuscript Author Manuscript Author Manuscript

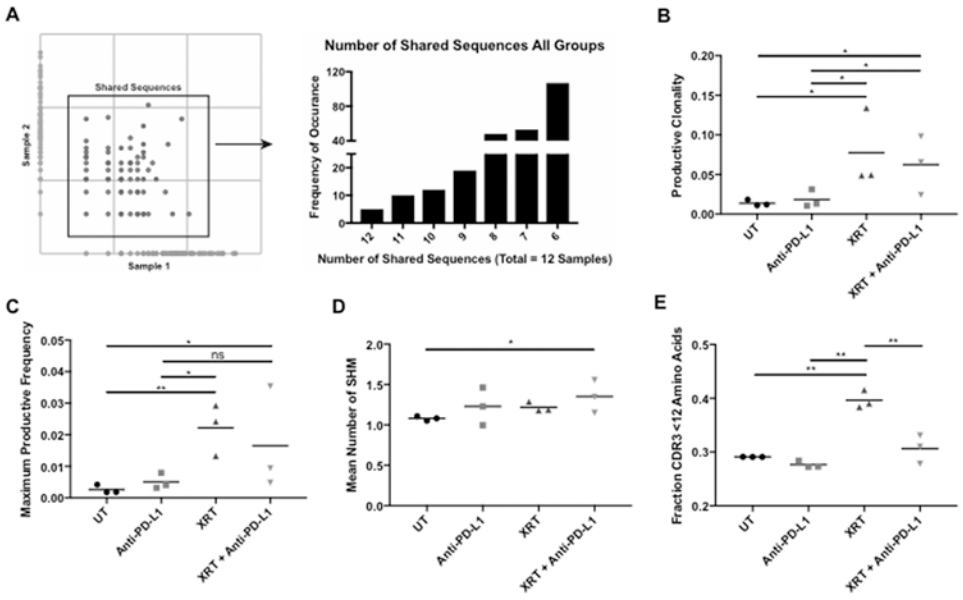

Figure 4: Anti-PD-L1 immunotherapy and radiation therapy enhance B-cell clonality and somatic hypermutation.

(A) Left, Representative scatterplot demonstrating BCR sequences found in the two or three distinct samples from TDLN; right, frequency of B cell clones occurring multiple TDLN samples. (B, C) Productive clonality (B) and maximum productive frequency (C) of B-cells in the TDLN. (D) Mean number of somatic hypermutations per productive BCR sequence in the TDLN. (E) Proportion of productive BCR templates in the TDLN that possess a CDR3 length of less than 12 amino acids.

Author Manuscript Author Manuscript Author Manuscript Author Manuscript

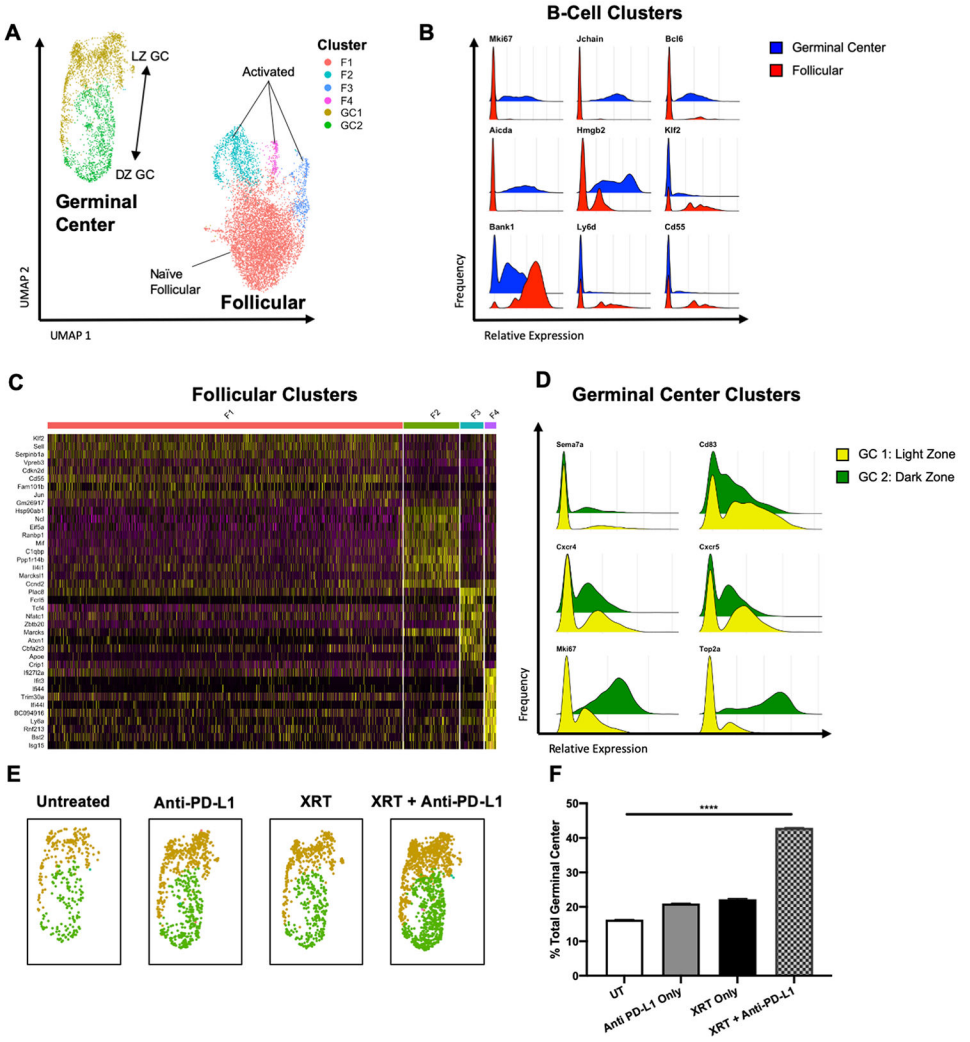

Figure 5: Single cell RNA sequencing demonstrates that radiation combined with anti-PD-L1 immunotherapy significantly enhances development of germinal center B-cells.

(A) UMAP plot of integrated analysis of sorted B-cells from the tumor-draining lymph node of tumor-bearing mice that were untreated, or treated with RT, anti-PD-L1 CBI, or combination therapy divided with clear clusters corresponding to follicular and germinal center (GC) B-cells. (B) Ridge plots demonstrating expression of select genes between the GC and follicular B-cell clusters. (C) Heat map demonstrating the expression profile of the top 10 most differentially expressed genes in each sub-cluster of follicular B-cells (clusters F1-F4). (D) Ridge plots demonstrating expression of select genes between two sub-clusters of GC B-cells corresponding to light zone (GC 1) and dark zone (GC 2). (E) UMAP plots of GC B-cells from individual treatment groups. (F) Proportion of total B-cells from each sample belonging combined germinal center clusters.

Author Manuscript Author Manuscript Author Manuscript Author Manuscript

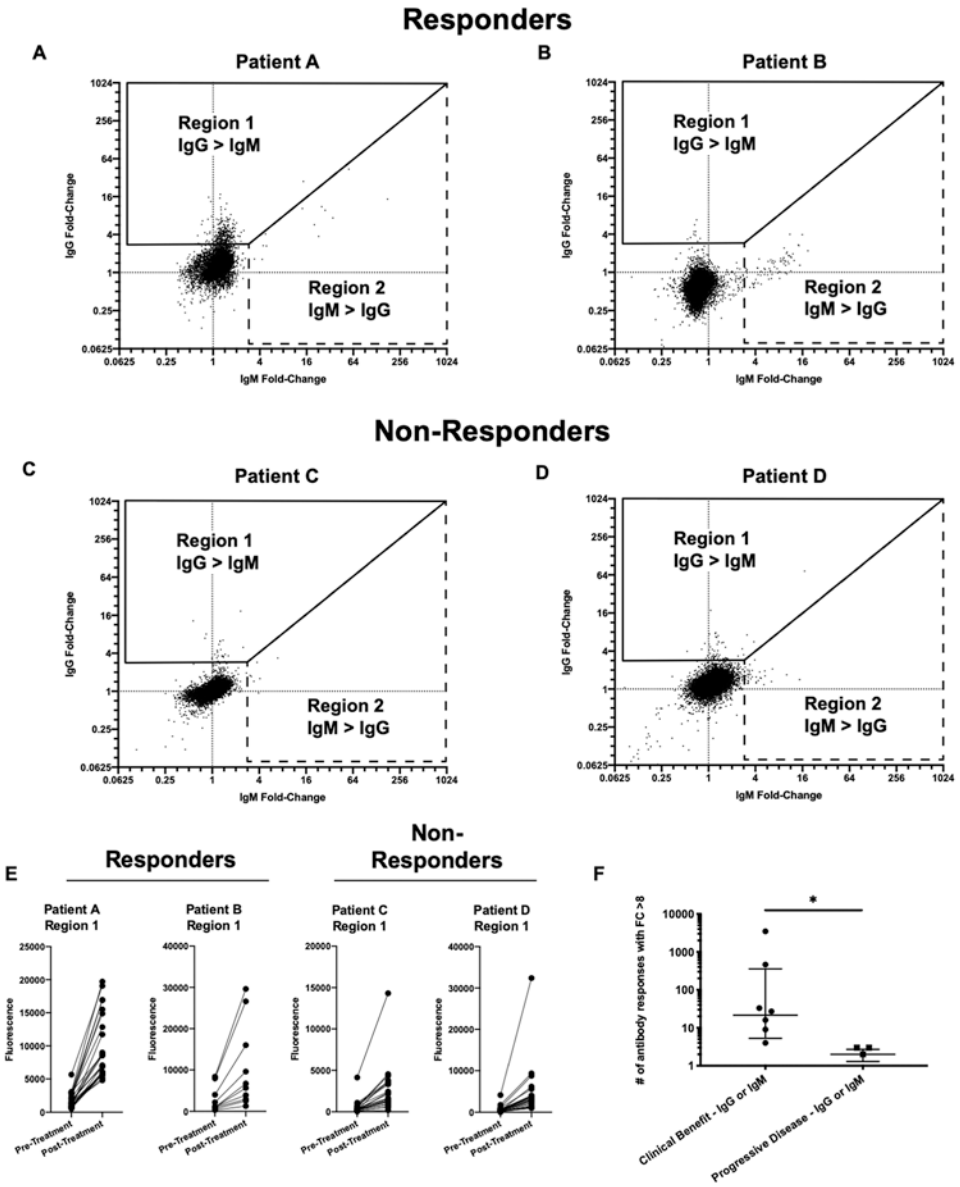

Figure 6: B-cell mediated IgG and IgM antibody responses correlate with objective responses to checkpoint blockade immunotherapy.

Representative plot of IgG and IgM antibody responses for all matched targets in patients treated with CBI +/− SBRT in patients with objective responses (A, B) and progressive disease (C, D). (E) Fluorescence values for top 25 of fewer IgG antibodies in region 1 for each patient shown. (F) Number of antibody responses with an IgG or IgM post-treatment fold-change greater than 8 in patients with clinical benefit versus progressive disease.